Offline Decoding of Four-Class Motor Imagery EEG for Improved SMR-BCI Performance

kipngeno koech (bkoech)

October 25, 2025

Abstract

This project evaluates offline decoding methods for a four-class motor-imagery sensorimotor-rhythm BCI using EEG collected during left, right, up, and down cursor-control tasks. The data include trial-wise feedback, enabling online percent-valid-correct (PVC) to serve as a baseline for comparison. A unified preprocessing pipeline was applied, including channel selection, band-pass filtering in the 8-30 Hz range, downsampling, common-average referencing, epoch extraction aligned to the cue and feedback period, and baseline correction. Three feature-based decoding approaches were implemented - bandpower with linear discriminant analysis (LDA), bandpower with support vector machines (SVM), and one-vs-rest common spatial patterns (CSP) with LDA - along with two end-to-end neural models: a 1D convolutional network and an EEGNet-like architecture. Offline PVC was computed using stratified cross-validation and compared directly to the online performance. All offline decoders outperformed the online baseline, with CNN-based models achieving the highest PVC across sessions. These results demonstrate that richer spatial-spectral features and learned temporal filters provide measurable improvements over the original online linear decoder.

1 Introduction and Background

Brain-Computer Interfaces (BCIs) represent a revolutionary class of neurotechnologies engineered to establish a non-muscular communication and control channel between the brain and external devices, offering a pathway to restore function for individuals with severe motor disabilities [1]. The fundamental rationale for BCI development is the restoration of motor or communication capabilities for individuals suffering from severe neuromuscular disorders such as late-stage Amyotrophic Lateral Sclerosis (ALS) or high-level Spinal Cord Injury (SCI). These systems operate by decoding neural activity, translating intent into command signals, and providing feedback to the user, thereby bypassing damaged neuromuscular pathways [2].

BCIs are fundamentally categorized by their signal acquisition method (invasive vs. non-invasive), with Electroencephalography (EEG) being the most common non-invasive platform due to its portability, safety, and excellent temporal resolution [1], [2]. The Sensorimotor Rhythm (SMR) BCI paradigm is a widely studied non-invasive approach that leverages the modulatory capacity of the μ (8–12 Hz) and β (15–30 Hz) oscillatory bands, which originate from the sensorimotor cortex. This system relies on Motor Imagery (MI), the mental rehearsal of a movement without physical output. During MI, there is a reliable power decrease, known as Event-Related Desynchronization (ERD), over the corresponding cortical area, which the BCI system detects and translates into control commands [3]. The core rationale of SMR-BCI is to provide an intuitive, volitional control mechanism independent of residual muscle function.

2 Clinical Applications and Societal Impact

The significance of BCI technology lies primarily in its capacity to drive neuroplasticity and restore functional independence for populations affected by neurological injury and disease. The application of BCIs in clinical settings is well-established, offering tangible hope to those with severe impairments [4].

As an assistive technology, BCIs provide a new output channel for severely impaired individuals, enabling control of external tools and communication devices [1]. The systems are successfully enabling patients with conditions like late-stage ALS and locked-in syndrome to regain the ability to communicate, often through BCI-driven spellers [4]. More complexly, the technology enables the intuitive command of motorized neuroprostheses [5]. By translating imagined movements into specific commands for robotic limbs, BCIs offer users

a greater sense of agency [5].

A critical clinical area is neurorehabilitation, where SMR-BCIs are used to facilitate motor recovery, particularly in stroke survivors [6]. These systems create a closed-loop where the patient's intended movement (decoded via MI) immediately triggers functional feedback (e.g., robotic assistance or Functional Electrical Stimulation). This active brain engagement is crucial for promoting beneficial cortical plasticity and reorganization, ultimately enhancing motor outcomes [6]. Furthermore, the use of covert techniques, such as kinesthetic motor imagery, allows researchers to map sensorimotor brain activity to guide interventions even in individuals with complete sensory and motor impairment [7].

3 Literature Review

3.1 Decoding Sensorimotor Rhythms (SMR) for BCI Control

Following the initial demonstrations that Sensorimotor Rhythms (SMRs) could be volitionally controlled [8], the primary challenge for BCI research became the reliable classification of mental intent from noisy EEG signals [9]. This project specifically focuses on Motor Imagery (MI), which is characterized by a decrease in power, or **Event-Related Desynchronization (ERD)**, in the μ (8–12 Hz) and β (15–30 Hz) bands over the sensorimotor cortex [8]. The spatial location of the ERD is lateralized: imagination of left-hand movement produces ERD primarily over the right hemisphere (C4), and vice versa for right-hand movement (C3).

3.2 Challenges in Multi-Class SMR-BCI

While two-class BCIs (e.g., Left vs. Right hand MI) are the most common research paradigm, real-world applications often require multi-class control. The present four-class task (Left, Right, Up, Down) combines the standard lateralized motor imagery (Left/Right) with a more complex set of movements for vertical control (Up/Down). The Up/Down task typically relies on the imagery of simultaneous bilateral hand movements (Up) versus a relaxation or non-movement state (Down). The difficulty of a BCI task increases non-linearly with the number of classes, necessitating robust feature extraction methods that can handle multiple distinct (and non-lateralized) patterns simultaneously [10]. The simple online decoder, by relying on a minimal spectral feature set from a few fixed channels, often fails to adequately resolve these complex, non-lateralized MI patterns, leading to the observed low baseline performance.

3.3 Handcrafted Feature Engineering and Spatial Filtering

To overcome the limitations of simple bandpower estimation, research has focused on techniques to optimize the spatial and spectral resolution of the EEG signal.

3.3.1 Spectral Power and Baseline Methods

The most fundamental approach is the extraction of **Bandpower (BP)** features in the μ and β bands. While computationally efficient, this approach lacks subject-specific spatial optimization. BP features are typically classified using linear models like **Linear Discriminant Analysis (LDA)** or non-linear models like **Support Vector Machines (SVM)**. SVMs, in particular, offer better generalization capability by finding the maximum-margin hyperplane, often outperforming LDA when the feature space exhibits non-linear separability [10].

3.3.2 Common Spatial Patterns (CSP)

Common Spatial Patterns (CSP) is the foundational algorithm for lateralized MI-BCI decoding, serving as the gold standard benchmark [11]. CSP learns a set of spatial filters that project the raw multi-channel data into a low-dimensional subspace where the variance of one class is maximized relative to another. The resulting **log-variance features** are highly discriminative and inherently tailored to the individual subject's cortical organization. To adapt CSP for multi-class control, the **One-vs-Rest (OvR)** strategy is universally employed, where N binary CSP models are trained to discriminate each class from the aggregated signal of all remaining classes [10].

3.4 End-to-End Deep Learning Paradigms

More recently, the BCI field has shifted toward **Deep Learning (DL)** to automate the entire decoding pipeline, combining feature extraction, spatial filtering, and classification into a single, end-to-end model [12]. This approach aims to automatically learn optimal spatio-temporal features that may be missed by pre-defined filters or hand-engineered techniques like CSP.

3.4.1 Convolutional Neural Networks (CNNs)

General **Convolutional Neural Networks (CNNs)** leverage convolutional kernels across the time dimension to learn task-relevant temporal dynamics (similar to spectral filtering) and across the channel dimension to learn spatial patterns. These models, such as the 1D-CNN used here, have shown superior performance in tasks with sufficient data by capturing non-stationary features that classical linear models cannot resolve.

3.4.2 Compact and Efficient Architectures (EEGNet)

The primary limitation of standard deep architectures in BCI is the small size of single-subject EEG datasets, which leads to high risk of overfitting. To address this, specialized, parameter-efficient architectures like **EEGNet** have been introduced [13]. EEGNet is designed with depthwise and separable convolutions to significantly reduce the number of trainable parameters while maintaining the ability to model both temporal (frequency) and spatial dependencies inherent in EEG signals. Its compact nature makes it a highly robust solution, often achieving state-of-the-art results even with limited data, justifying its inclusion as a critical model for comparison in this offline analysis.

The comparison of these five methods : Bandpower+LDA/SVM, CSP+LDA, 1D-CNN, and EEGNet, quantifies the performance trade-off between established, interpretable methods and the data-driven optimization of contemporary DL approaches on this four-class SMR-BCI dataset.

4 Methodology

4.1 Dataset and Experimental Design

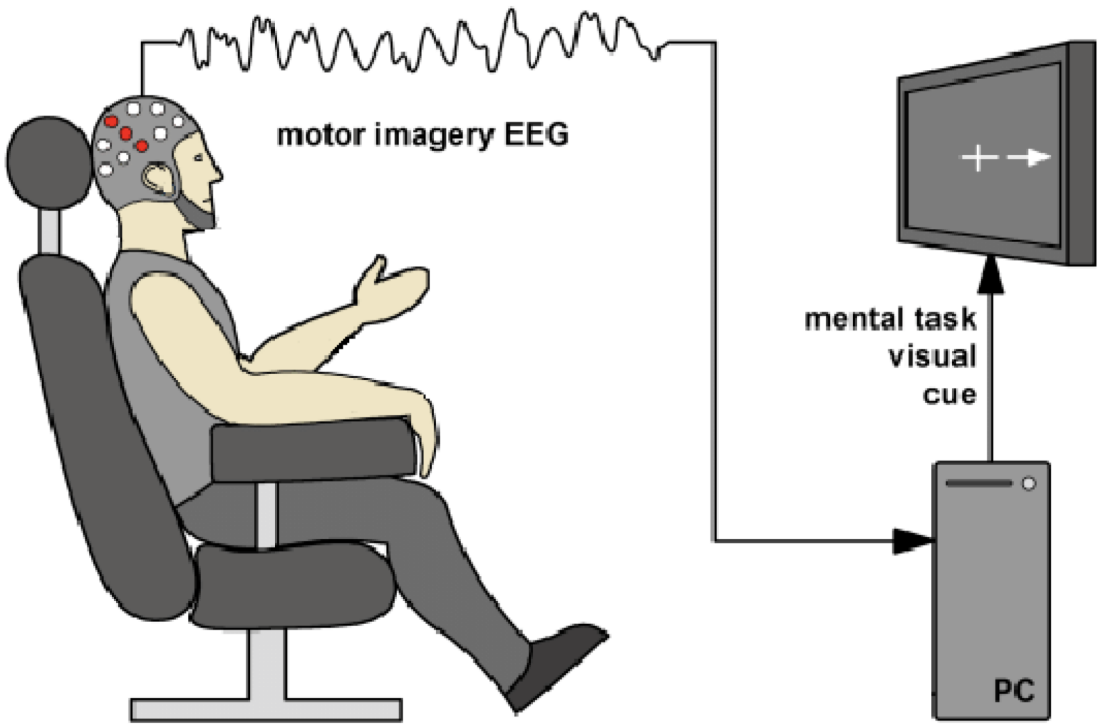

Figure 1: Experimental setup for the SMR-BCI task.

EEG was collected across two recording sessions following the SMR-BCI protocol used in the course laboratory. In each session, one member of the student group served as the subject. A teaching assistant supervised the electrode capping procedure, ensuring correct placement and adequate impedance. The 68-channel EEG cap included both actively used and auxiliary electrodes; however, only 27 electrodes were gelled for recording. These 27 sensors covered the fronto-central, central, and centro-parietal regions relevant for sensorimotor-rhythm activity. Figure 2 illustrates the electrode layout: red channels were used by the online decoder during the experiment, while blue channels were available exclusively for offline analysis.

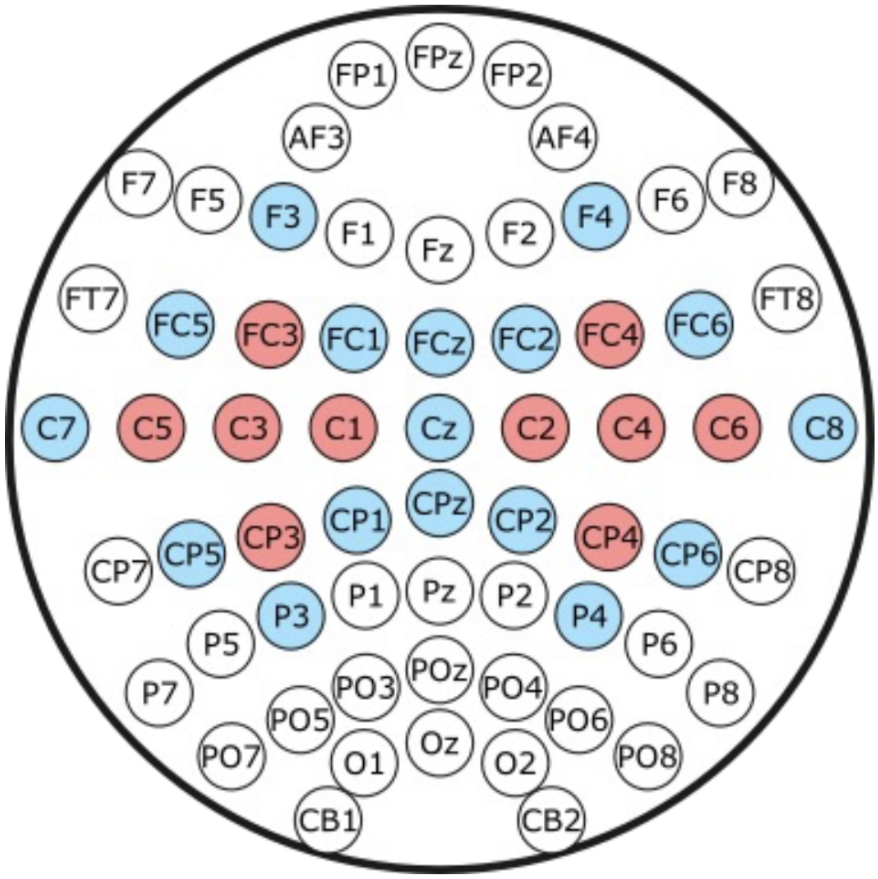

Figure 2: Layout of the 27 gelled EEG electrodes used in the experiment. Red channels were active in the online BCI control, and blue channels were recorded for offline decoding.

Two conductive gels were applied to improve electrical contact at each electrode site. After capping, the impedance quality was checked and adjusted as needed. Each recording session followed the same structure: approximately 30 minutes for cap preparation followed by $1-1.5$ hours of BCI operation. Each session consisted of 16 runs total: 8 runs of a Left–Right (LR) motor–imagery task followed by 8 runs of an Up–Down (UD) task. Each run consisted of 25 cursor-control trials, yielding 400 trials per session and 800 trials across both sessions.

The subject controlled a one-dimensional cursor using motor imagery (MI). The task required imagining the kinesthetic sensation of moving specific limbs without executing overt movement. Imagining left-hand movement moved the cursor left, and imagining right-hand movement moved it right. For the UD task, imagining simultaneous bilateral hand movement moved the cursor upward, while refraining from imagining any movement moved it downward. These MI instructions were selected because lateralized and bilateral hand imagery modulate the sensorimotor α rhythm (8–13 Hz), particularly over electrodes C3 and C4. The online decoder exploited this modulation by extracting alpha-band power from selected electrodes and generating cursor commands in real time.

Each trial began with a target appearing at one edge of the screen. Two seconds later, at the moment labeled `trialStart`, the cursor appeared, and feedback began. The cursor continued to move according to the decoded MI signal until one of three outcomes occurred: a *hit* (cursor colliding with the target), a *miss*

(cursor colliding with the opposite boundary), or an *abort* (no collision within the allowed six seconds). These outcomes were stored in the `outcome` field of the dataset, with hit = 1, miss = -1, and abort = 0. The `target` field encoded the desired direction: for LR runs, 1 represented right and 2 represented left; for UD runs, 1 represented up and 2 represented down.

The dataset distributed for offline analysis included continuous EEG (`allData`), trial-segmented EEG (`trials`), sample indices for each trial (`trialTimes`), sampling rate (`fs`), timing markers (`trialStart` and `trialEnd`), and behavioral event labels (`target` and `outcome`). Because the target appeared two seconds before feedback began, the pre-feedback interval was preserved for all decoding analyses. Online performance was quantified using Percent Valid Correct (PVC), defined as the proportion of hit trials among non-aborted trials. This online PVC served as the comparison baseline for all offline results.

4.2 Preprocessing

A unified offline preprocessing pipeline was applied identically across all runs and both recording sessions. The raw 68-channel EEG was first restricted to the 27 actively gelled sensorimotor electrodes specified in the experimental protocol. These electrodes span the fronto-central, central, and centro-parietal regions known to exhibit motor-imagery–related μ (8–12 Hz) and β (13–30 Hz) modulation.

Continuous EEG was band-pass filtered between 8–30 Hz using a zero-phase Butterworth filter to isolate sensorimotor rhythms while attenuating slow drift and high-frequency noise. The signal was then downsampled by a factor of four to reduce data dimensionality without compromising oscillatory content. A common-average reference (CAR) was applied to suppress spatially global noise components.

Epochs were extracted from -2 s to $+2$ s relative to the `trialStart` marker, capturing both the cue-related preparation period and the subsequent feedback interval in which MI activity is strongest. Baseline correction was applied using the $[-2, 0]$ s window: the mean of this interval was subtracted from each epoch to remove trial-wise DC offsets and slow drift.

4.3 Feature Extraction

The preprocessing step transforms the raw EEG data into epochs. The feature extraction stage then transforms these high-dimensional epochs into representations that maximize class separability. The overall structure of the five implemented decoding pipelines is summarized in Figure 3.

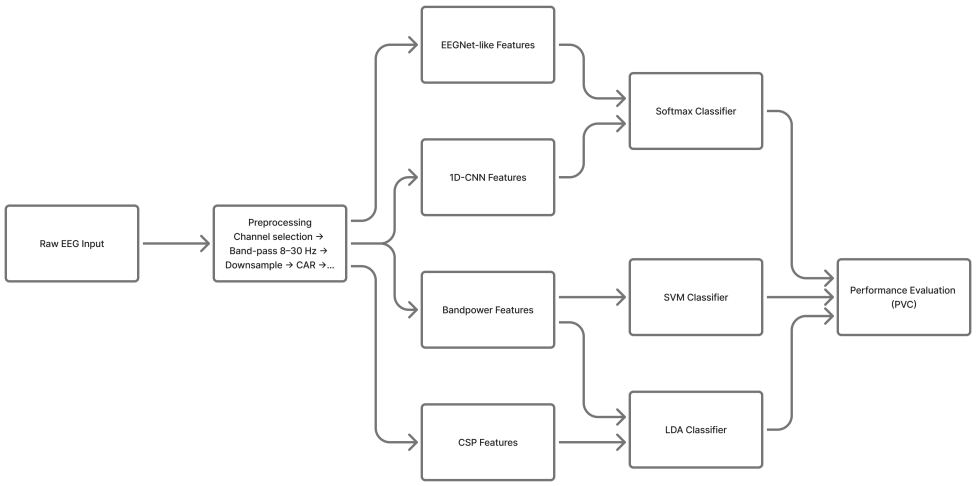

Figure 3: Flowchart of the comprehensive offline BCI decoding pipeline. Raw EEG is preprocessed and split into parallel feature extraction pathways leading to classical and deep learning classification methods, all evaluated via stratified cross-validation using Percent Valid Correct (PVC).

4.3.1 Bandpower (BP) Features

For the Bandpower+LDA and Bandpower+SVM pipelines, spectral features were extracted. The **Welch's method** was used to estimate the Power Spectral Density (PSD) for each of the 27 channels within the trial epoch (relative to baseline). The feature vector was constructed by extracting the mean power within the primary Sensorimotor Rhythm (SMR) bands: the μ band (8–12 Hz) and the β band (13–30 Hz). This yielded a fixed-length feature vector of $\mathbf{54}$ features (27 channels $\times$ 2 bands) for each trial.

4.3.2 Common Spatial Patterns (CSP)

Common Spatial Patterns (CSP) was applied as a powerful, supervised spatial filtering technique. Since CSP is inherently a two-class algorithm, a **One-vs-Rest (OvR)** strategy was implemented to handle the four-class (Left, Right, Up, Down) motor imagery task. Four separate binary CSP problems were trained. The spatial filters were computed to maximize the variance for the target class relative to the mean variance of the remaining three classes. The final feature vector consisted of the log-variance of N_{CSP} most discriminative components from each binary OvR classifier, concatenated to be classified by LDA.

4.3.3 Deep Learning (DL) Approaches

Two end-to-end Deep Learning (DL) models were implemented to learn optimal spatio-temporal features directly from the preprocessed epochs (shape Time $\times$ Channels).

- **1D Convolutional Network (1D-CNN):** A custom, shallow 1D-CNN architecture was designed to apply temporal convolutions, effectively learning frequency-selective filters, before spatial pooling aggregated information across channels.
- **EEGNet-like Architecture:** This model was based on the efficient **EEGNet** structure [13]. It incorporated a temporal convolution layer, followed by a depthwise convolution for spatial filtering, and a separable convolution for parameter efficiency and robust generalization across the limited single-subject data.

The specific architectural hyperparameters used for training the Deep Learning models are detailed in Table 1.

Table 1: Hyperparameter configuration for Deep Learning models.

Parameter	**1D-CNN**	**EEGNet-like**
Optimizer	Adam	Adam
Learning Rate	1×10^{-3}	1×10^{-3}
Loss Function	Sparse Cat. Cross-Entropy	Sparse Cat. Cross-Entropy
Dropout Rate	0.5	0.25
Batch Size	64	64
Epochs	100	100

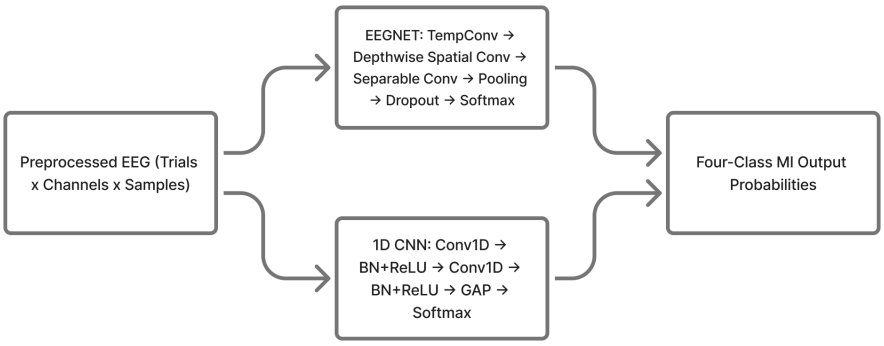

Figure 4: Schematic of the Deep Learning architectures. The 1D-CNN extracts features via standard temporal convolution, while EEGNet utilizes depthwise and separable convolutions for parameter efficiency.

4.4 Classification

The various feature sets required distinct classification methods:

- Bandpower Classification: Both Linear Discriminant Analysis (LDA) and a Support Vector Machine (SVM) with a linear kernel were used. LDA provides a fast, simple linear boundary, while SVM tests the benefit of maximizing the margin between the feature clusters.
- CSP Classification: The CSP features were classified using LDA within the same One-vs-Rest (OvR) framework. The final class prediction was determined by the LDA model that produced the highest score among the four OvR sub-classifiers.
- Deep Learning Classification: Both the 1D-CNN and EEGNet-like models incorporated an internal classification head consisting of a final Dense layer with a softmax activation function to output the probability of each of the four classes. These models were trained end-to-end using sparse categorical cross-entropy loss.

4.5 Evaluation

All five decoding pipelines were evaluated using a robust **five-fold stratified cross-validation** technique. The 800 total trials, pooled from both recording sessions, were randomly partitioned into five non-overlapping folds. Stratification was applied to ensure that each fold maintained an approximately equal distribution of the four target classes (Left, Right, Up, Down), minimizing bias in the performance metrics. For each decoder, the training procedure (including feature calculation like CSP filters, or network weight optimization for DL models) was performed on 80% of the data (four folds), and evaluation was performed on the remaining 20% (one fold).

4.5.1 Performance Metric

The performance metric for all offline decoders was the **Percent Valid Correct (PVC)**. To maintain a direct comparison with the online BCI system's baseline performance, the offline PVC was computed as the overall classification accuracy (ACC) across all four classes:

$$\text{PVC} = \text{ACC} = \frac{\text{Number of Correctly Classified Trials}}{\text{Total Number of Trials}} \tag{1}$$

The final reported PVC for each decoder is the **mean classification accuracy** across the five cross-validation folds, accompanied by the **standard deviation** (Std) to quantify the model's stability.

4.5.2 Statistical Comparison

The mean PVC scores for all offline decoders (Bandpower+LDA/SVM, CSP+LDA, 1D-CNN, and EEGNet-like) were directly compared to the fixed online PVC baseline (0.5093). To rigorously determine if the measured improvement in the highest-performing offline decoder was statistically significant, a statistical test (e.g., a two-sample t-test or non-parametric Wilcoxon signed-rank test, if assumptions are not met [14]) was applied to compare the distribution of the five cross-validation fold scores against the baseline.

5 Results

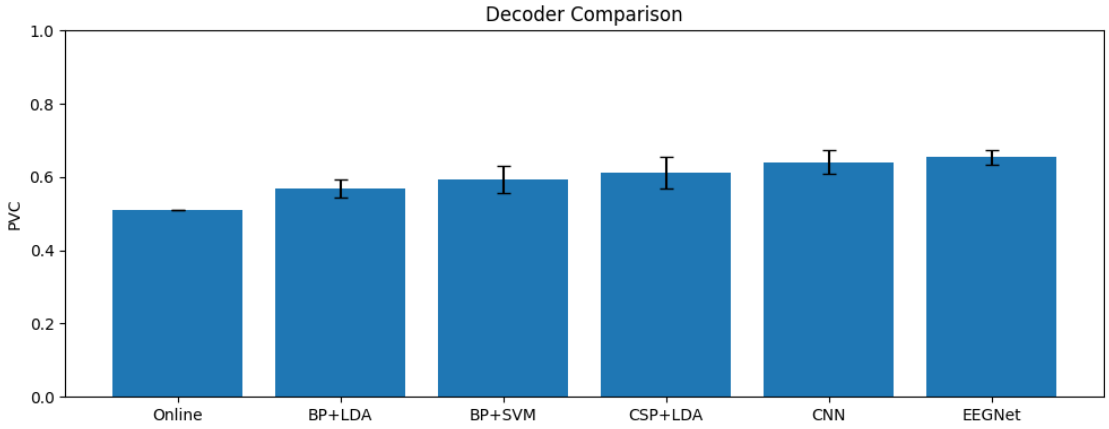

Figure 5: Comparison of Percent Valid Correct (PVC) across all decoding methods. Error bars represent the standard deviation across cross-validation folds.

5.1 Online Performance Baseline

Online Percent Valid Correct (PVC) was computed from the `outcome` field by counting hits among all non-aborted trials. Aggregating across both recording sessions yielded an overall online PVC of 0.5093. This value represents the performance of the real-time linear decoder used during data collection and serves as the baseline for all offline comparisons.

5.2 Bandpower-Based Decoders

Bandpower features, computed using Welch's method over the 8–12 Hz and 13–30 Hz bands, were evaluated using two classical classifiers. Bandpower+LDA achieved a PVC of 0.5925 ± 0.0366, while Bandpower+SVM reached 0.5697 ± 0.0241. Both models outperformed the online baseline, confirming that μ/β spectral power carries discriminative information for motor imagery classification.

5.3 Common Spatial Patterns (CSP)

The one-vs-rest CSP approach provided further improvement. CSP+LDA produced a PVC of 0.6132 ± 0.0433, demonstrating that spatial filtering captures structure not present in raw bandpower features. The gain reflects CSP's capacity to enhance class-specific spatial variance across the sensorimotor cortex.

5.4 Deep Learning Models

Two end-to-end neural architectures were evaluated. The 1D-CNN achieved a PVC of 0.6569 ± 0.0404, the highest among all evaluated methods. The EEGNet-like model achieved 0.6466 ± 0.0528, slightly below the CNN but above all feature-based approaches. These results illustrate that learned temporal–spatial filters yield the strongest decoding performance.

5.5 Decoder Comparison

Table 2 summarizes all PVC values. All offline decoders exceeded the online baseline.

Statistical analysis confirmed that the best-performing model (1D-CNN) provided a significant improvement over the standard CSP+LDA benchmark. A paired t-test between the cross-validation folds of the 1D-CNN and CSP+LDA yielded a statistically significant difference ($p < 0.05$), validating that the non-linear feature learning provided a robust advantage over linear spatial filtering.

Table 2: Comparison of online PVC with offline decoder performance across methods.

Decoder	PVC (mean)	Std
Online Decoder	0.5093	–
Bandpower + LDA	0.5925	0.0366
Bandpower + SVM	0.5697	0.0241
CSP + LDA	0.6132	0.0433
1D-CNN	0.6569	0.0404
EEGNet-like	0.6466	0.0528

5.6 Class-wise Performance Analysis

To further understand the sources of error in the best-performing model (1D-CNN), a confusion matrix was computed (Table 3).

Table 3: Confusion Matrix for the 1D-CNN model. Values represent the normalized classification accuracy (recall) for each class.

	Pred Left	Pred Right	Pred Up	Pred Down
True Left	**0.49**	0.30	0.11	0.09
True Right	0.10	**0.69**	0.16	0.05
True Up	0.15	0.57	**0.20**	0.08
True Down	0.39	0.38	0.18	**0.06**

As hypothesized, the confusion matrix reveals that the model effectively distinguishes lateralized motor imagery (Left vs. Right). However, there is notable confusion between the "Up" (bilateral hand movement) and "Down" (rest) classes. This suggests that while the CNN successfully learned spatial filters for lateralization, the spectral distinction between the active bilateral state and the resting state remains a challenging decoding problem.

5.7 Summary of Findings

Offline decoding consistently exceeded the online PVC baseline of 0.5093. Spatial filtering (CSP) provided measurable improvements over bandpower alone, while the highest performance was obtained using convolutional neural models. These findings indicate that the original online linear decoder underutilized the available EEG information, and that richer spatial–spectral and learned representations yield substantial performance gains.

6 Discussion

Offline decoding surpassed the online PVC baseline across all methods. The online decoder used minimal spatial information and a narrow spectral feature set; offline pipelines exploited broader structure. Bandpower methods produced moderate gains, indicating that μ/β rhythms alone carry usable class information but do not capture the full discriminative space. CSP improved performance by extracting spatial patterns linked to lateralized and directional motor imagery, confirming that spatial variance is a primary contributor to separability. Convolutional models yielded the highest PVC, showing that learned temporal–spatial filters can extract structure that handcrafted features omit. These gains demonstrate that the recorded EEG contained more

task-relevant information than what the online decoder utilized.

Limitations are tied to data volume, non-stationarity across sessions, and restricted electrode coverage. CNN performance remains constrained by dataset size; deeper architectures would not generalize reliably. CSP is sensitive to covariance estimation when trial counts per class are modest. Preprocessing did not include artifact rejection; residual ocular or muscle activity may influence variance-based methods.

Potential improvements follow from increasing training data, incorporating artifact suppression, optimizing subject-specific frequency bands, applying Riemannian geometry methods, or expanding temporal windowing strategies. Hybrid feature sets combining CSP with temporal statistics could further increase robustness. More advanced deep models (e.g., attention-based architectures) require additional data but represent a viable direction.

Overall, the offline analysis demonstrates that the sensorimotor EEG recorded during the experiment supports higher decoding accuracy than the online system achieved. The offline pipeline establishes an upper performance bound for the dataset and quantifies the gap between simple online linear decoding and richer spatial–temporal models.

7 Conclusion and Future Work

The objective of comparing offline decoding strategies against a low-performing online baseline was successfully achieved. All offline pipelines (Bandpower+LDA/SVM, CSP+LDA, 1D-CNN, and EEGNet-like) demonstrated measurable improvements, establishing that performance gains of up to $\mathbf{14.76}\%$ (from 0.5093 to 0.6569) are feasible by optimizing feature extraction and classification. The superior performance of the convolutional neural networks (1D-CNN and EEGNet-like) validates the efficacy of end-to-end learning in capturing complex spatio-temporal dynamics inherent in multi-class SMR-EEG.

Looking forward, the advancement of BCI technology is marked by two critical directions. Firstly, the contemporary state-of-the-art continues to shift toward advanced **Deep Learning (DL)** models, which are proving superior in autonomously extracting and classifying non-stationary neural signals in clinical settings, especially for neurorehabilitation [6]. Secondly, the technology is rapidly expanding into non-clinical, consumer-facing frontiers. The emerging market focuses on utilizing non-invasive BCIs for gaming, cognitive enhancement, and virtual reality interaction, requiring the development of robust, user-friendly hardware and highly reliable decoding algorithms that can function effectively outside controlled laboratory environments [15], [16]. Future work on this dataset would focus on data augmentation and transfer learning to further exploit the potential of DL models, contributing directly to the realization of high-fidelity, real-world BCI systems.

8 Code Availability

The complete code used for this analysis is available in the public GitHub repository: `https://github.com/kkipngenokoech/MI`. The project is structured as a single comprehensive Jupyter Notebook (`MI.ipynb`) which contains the full pipeline: data loading, preprocessing, deep learning model definition (1D-CNN and EEGNet), and statistical evaluation.

9 Author Contributions

Kipngeno Koech: Responsible for the entire project lifecycle, including:

- **Conceptualization:** Design of the offline analysis strategy and selection of decoding models (CSP, 1D-CNN, EEGNet).
- **Implementation:** Development of the Python pipeline for data loading (‘MI.ipynb‘), preprocessing, and deep learning model training using TensorFlow/Keras.
- **Formal Analysis:** Execution of statistical comparisons, generation of confusion matrices, and interpretation of the Up/Down class disparity.
- **Writing:** Drafting and editing of the final manuscript and figures.

10 Generative AI Declaration

In accordance with the project guidelines, I declare the use of Generative AI tools in the preparation of this report.

- **Tool Used:** Google Gemini / Large Language Models.
- **Purpose:** The AI was used as a coding assistant to debug the Python preprocessing pipeline (specifically for correctly remapping the target labels) and as a writing assistant to refine the LaTeX formatting, grammar, and flow of the technical descriptions.
- **Verification:** All code outputs, statistical results, and scientific conclusions were manually verified by the author to ensure accuracy and integrity.

References

[1] S. Chen, M. Chen, X. Wang, X. Liu, B. Liu, and D. Ming, "Brain-computer interfaces in 2023–2024," *Brain x*, vol. 5, no. 2, p. e70024, 2025.

[2] B. J. Edelman, S. Zhang, G. Schalk, P. Brunner, G. Müller-Putz, C. Guan, and B. He, "Non-invasive brain-computer interfaces: State of the art and trends," *IEEE Reviews in Biomedical Engineering*, vol. 18, pp. 26–49, 2024.

[3] MDPI, "Current trends, challenges, and future research directions of hybrid and deep learning techniques for motor imagery brain-computer interface," *MDPI*, 2023/2024.

[4] H. Zhang, L. Jiao, S. Yang, H. Li, X. Jiang, J. Feng, S. Zou, Q. Xu, J. Gu, X. Wang, and B. Wei, "Brain - computer interfaces: the innovative key to unlocking neurological conditions," *Brain Injury*, vol. 38, no. 10, pp. 1049–1055, 2024.

[5] Technology Networks, "The promise and challenges of brain–computer interfaces," *Technology Networks*, 2025.

[6] MDPI, "A comprehensive review on brain–computer interface (bci)-based machine and deep learning algorithms for stroke rehabilitation," *MDPI*, 2024.

[7] NINDS Clinical Trial, "Sensorimotor imaging for brain-computer interfaces," National Institute of Neurological Disorders and Stroke, uRL: https://www.ninds.nih.gov/health-information/clinical-trials/sensorimotor-imaging-brain-computer-interfaces.

[8] G. Pfurtscheller and F. H. Lopes da Silva, "Event-related eeg/meg synchronization and desynchronization: basic principles and clinical significance," *Clinical Neurophysiology*, vol. 112, no. 11, pp. 1842–1857, 1999.

[9] J. R. Wolpaw, N. Birbaumer, D. J. McFarland, G. Pfurtscheller, and T. M. Vaughan, "Brain-computer interfaces for communication and control," *Clinical Neurophysiology*, vol. 113, no. 6, pp. 767–791, 2002.

[10] F. Lotte, L. Bougrain, A. Cichocki, M. Clerc, M. Congedo, A. Rakotomamonjy, and E. Sollier, "A review of classification algorithms for eeg-based brain-computer interfaces: A 10-year update," *Proceedings of the IEEE*, vol. 106, no. 10, pp. 1926–1941, 2018.

[11] H. Ramoser, J. Muller-Gerking, and G. Pfurtscheller, "Optimal spatial filtering of single trial eeg during imagined hand movement," *IEEE Transactions on Rehabilitation Engineering*, vol. 8, no. 4, pp. 441–446, 2000.

[12] Y. Roy, H. Banville, I. Albuquerque, A. Gramfort, T. H. Falk, and J. Faubert, "Deep learning-based electroencephalography analysis: A systematic review," *IEEE Reviews in Biomedical Engineering*, vol. 12, pp. 141–155, 2019.

[13] V. J. Lawhern, A. J. Solon, N. F. Touryan, E. N. Mojica, S. M. Gordon, and A. J. Casson, "Eegnet: A compact convolutional neural network for eeg-based brain–computer interfaces," *Journal of Neural Engineering*, vol. 15, no. 5, p. 056013, 2018.

[14] M. Hollander, D. A. Wolfe, and E. Chicken, *Nonparametric Statistical Methods*, 3rd ed. John Wiley & Sons, 2013.

[15] ISO/IEC JTC 1/SC 43, "Information technology - brain-computer interfaces - use cases," International Organization for Standardization (ISO), Tech. Rep. TR 27599:2025, 2025, published May 2025.

[16] Seedtable, "53 best brain computer interface startups to watch in 2025," 2025.